Chapter 8
Microstructure in Plasticity, a Comparison between Theory and Experiment

Olga Dmitrieva, Dierk Raabe, Stefan Müller, and Patrick W. Dondl

Abstract. We review aspects of pattern formation in plastically deformed single crystals, in particular as described in the investigation of a copper single crystal shear experiment in [DDMR09]. In this experiment, the specimen showed a band-like microstructure consisting of alternating crystal orientations. Such a formation of microstructure is often linked to a lack of convexity in the free energy describing the system. The specific parameters of the observed bands, namely the relative crystal orientation as well as the normal direction of the band layering, are thus compared to the predictions of the theory of kinematically compatible microstructure oscillating between low-energy states of the non-convex energy. We conclude that this theory is suitable to describe the experimentally observed band-like structure. Furthermore, we link these findings to the models used in studies of relaxation and evolution of microstructure.

8.1 Introduction

Plastically deformed single crystals often exhibit the formation of complex microstructure [BHHK92, Han90, HBO10], where dislocations in the crystal

Olga Dmitrieva · Dierk Raabe
Max-Planck-Institut fuer Eisenforschung, Duesseldorf, Germany
e-mail: {dmitrieva,raabe}@mpie.de

Stefan Müller
Hausdorff Center for Mathematics and Institute for Applied Mathematics, University Bonn, Bonn, Germany
e-mail: stefan.mueller@hcm.uni-bonn.de

Patrick W. Dondl
Department of Mathematical Sciences, Durham University, Durham, UK
e-mail: patrick.dondl@durham.ac.uk

S. Conti and K. Hackl (eds.), *Analysis and Computation of Microstructure in Finite Plasticity*, Lecture Notes in Applied and Computational Mechanics 78, DOI: 10.1007/978-3-319-18242-1_8

arrange in intricate patterns. Since the creation and propagation of dislocations ultimately mediates the plastic behavior of crystals, and these dislocations interact through the elastic field and the local lattice distortion they generate over many length scales, understanding the macroscopic plastic behavior of crystalline specimen is strongly dependent on understanding the microstructure formation.

The seminal work by Ortiz and Repetto [OR99] introduced an incremental implicit time-stepping approach in order to study the evolution of plastic deformation. In this approach, in each time-step, the sum of the stored elastic energy and an incremental dissipation is minimized. The elastic energy is usually assumed to be polyconvex, the dissipation in single crystals, however, is naturally non-convex: plastic deformation is easier in single-slip since otherwise sessile atomistic products of dislocations on different slip planes—so-called Lomer-Cottrell locks—form [RP99]. This non-convexity of the dissipation potential due to latent- (or cross-)hardening is a candidate for the description of plastic microstructure. Basically, the homogeneously deformed state becomes energetically unfavourable, so the plastic strain oscillates between favourable energy wells in the dissipation potential, i.e., states of single slip. This, however, can create long-range elastic effects which can only be avoided if the generated microstructure is kinematically compatible, in the sense that the plastic strain is the gradient of a continuous deformation. This links the study of plastic microstructure to the study of Martensitic phase transformations in shape-memory materials, where a non-convexity in the elastic energy (due to the underlying phase transformation) is the source of microstructure [BJ87]. In this context of phase transformations, sharply delineated, laminated, zones of alternating deformation states are often observed. At first glance, these laminates bear a striking resemblance to some of the microstructure seen in experiments in single-crystal plasticity.

In [OR99], there is already a number of experimental studies referenced in order to link such kinematically compatible laminates to observed plastic microstructure in a more rigorous manner [RP80, JW84]. Many of these experiments, however, were performed in fatigue, i.e., using repeated oscillating small amplitude plastic deformation. The goal in [DDMR09] was to examine the pattern formation in a well-controlled single pass shear experiment, thus bringing it closer to applications in deep-drawing and related industrial deformation methods.

The remainder of this chapter is organized as follows. In section 8.2 we will briefly review some approaches to the continuum modeling of microstructure in crystal plasticity. Section 8.3 describes the experiment from [DDMR09]. We then offer some conclusions in the final section 8.4.

8.2 Modeling Continuum Plasticity

The goal of this chapter is to test the underlying modeling assumptions that are used, for example, in the studies of energy relaxation in [CDK13b, CDK13a, CDK11, ACD09, CDK09] and in the studies of plastic evolution [HHK12, HK11, KH11] in continuum plasticity. We thus consider, in the framework of multiplicative continuum plasticity, a deformation $y\colon \Omega \to \mathbb{R}^3$, for $\Omega \subset \mathbb{R}^3$, with appropriate boundary conditions. The deformation gradient $F = \nabla y$ is decomposed multiplicatively into an elastic contribution and a purely plastic part (neither of which necessarily have to be kinematically compatible) as

$$F = F_{\mathrm{el}} F_{\mathrm{pl}}.$$

For further discussion on the subject of multiplicative strain decomposition see [RC14]. As mentioned in the introduction, we follow the approach by Ortiz and Repetto [OR99] in studying a time-discrete problem instead of a continuous time evolution problem. We will furthermore restrict ourselves here to the analysis of microstructure formation in a single time step. A suitable functional for such a time step now reads, with a suitable elastic energy density W_{el} and a plastic dissipation W_{pl},

$$E(y, F_{\mathrm{pl}}) = \int_\Omega W_{\mathrm{el}}(F_{\mathrm{el}}) + \int_\Omega W_{\mathrm{pl}}(F_{\mathrm{pl}}). \tag{8.1}$$

The assumption of strong latent hardening now leads to the assumption that the plastic deformation necessarily has to occur in single slip only. Given a set $\{m_j\}_{j=1}^M$ slip plane normals in the crystal and a set $\{b_{ij}\}_{i=1}^{N_j}$ Burgers' vectors (orthogonal to m_j, respectively) in each slip plane, we thus assume that

$$W_{\mathrm{pl}} = \begin{cases} 0 & \text{if } F_{\mathrm{pl}} = \mathrm{Id} + \sum_{j=1}^{M} \sum_{i=1}^{N_j} \gamma_{ij} b_{ij} \otimes m_j, \\ & \text{with } \gamma_{ij}\gamma_{kl} = 0 \text{ for } i \neq k \text{ or } j \neq l, \\ +\infty & \text{otherwise,} \end{cases}$$

where we have (for simplicity) disregarded dissipation, which is small for plastic deformation in single slip and introduced the single-slip side condition as an infinite penalty on the energy. We remark that we expect that our results in section 8.3 below would not change substantially if this side condition was made somewhat less strict by introducing a hardening matrix with large off-diagonal entries instead.

Commonly, a higher-gradient curl-type term is introduced to such an energy in order to account for geometrically necessary dislocations [Nye53, Kon52, CG01]. Even with such an additional regularization (certainly also without), one relaxation of the model that can immediately be performed is that of considering a single-plane side condition instead of the single-slip condition above. See [AD14] for more information. After this relaxation, the plastic dissipation can be written as

$$W_{\mathrm{pl}} = \begin{cases} 0 & \text{if } F_{\mathrm{pl}} = \mathrm{Id} + \sum_{j=1}^{M} s_j \otimes m_j, \\ & \text{with } s_j \in m_j^{\perp} \text{ and } |s_j|\,|s_l| = 0 \text{ for } j \neq l, \\ +\infty & \text{otherwise,} \end{cases} \tag{8.2}$$

The investigations in the aforementioned articles usually start with an energy of this kind, often assuming a limited number of slip systems (i.e., one or two) and then studying further relaxation, evolution, or computational problems [MRF10].

Our approach, as mentioned above, was somewhat different but complementary: we wanted to check whether a configuration admitting low energy can be found that reproduces observed microstructure. The experiment performed and its outcome are described in the following section.

8.3 A Single-Pass Shear Deformation Experiment and the Resulting Microstructure

This section is a review of material published in [DDMR09] and [DSDR10]. We briefly recapitulate the experimental methods and observations and then answer the question posed at the end of section 8.2 by explicitly constructing a low-energy microstructure that reproduces the experimentally observed parameters.

8.3.1 Sample Preparation and Shear Deformation Experiments

The specimens were cut by spark erosion from 99.98% pure copper single crystals produced by the melt-grow method to a dimension of 3 mm × 2 mm with a height of $10 - 15$ mm. They were then polished, first mechanically and finally electrolytically. The specimen is illustrated in Fig. 8.1a.

The shear experiments were performed on a special miniaturized testing device made by Kammrath Weiss GmbH (44141 Dortmund, Germany). The specimen is fixed in a stable, centered position between two movable cross-heads in the device. These cross-heads were sheared with respect to each other at a rate of 5 μm/s as measured by the machine extensometer, the load was controlled to a maximal load value of 1 kN by the device's load cell. For a schematic of the position of the specimen in the device see Fig. 8.1a. As seen in the figure, the freestanding part of the specimen has a length of 2.4 mm.

To an accuracy of 0.5°, the orientation of the undeformed single crystal specimen in the device is $(101)[12\bar{1}]$ with the shear load applied along the $[12\bar{1}]$ direction. Fig. 8.1b shows the shear load with respect to the crystal orientation in the context of the relevant f.c.c. slip systems in the {111}-plane given by

the normal of the applied shear load. Under the given loading conditions, there are two primarily active coplanar slip systems with Schmid factors of maximal magnitude.

8.3.2 Digital Image Correlation for Strain Mapping and EBSD for Texture Mapping

In the course of the shear deformation, the strain on the surface of the sample was measured using the digital image correlation (DIC) method. The basic idea of this method is that an optical pattern (graphite spray for optical decoration on white acrylic spray) is applied to the surface of the sample and geometrical changes of this pattern are recognized by means of digital image analysis. For DIC we used a GOM Inc. Aramis System (version 6.0.0-3) with two digital cameras (CCD-1300, maximal resolution 1280 × 1024 pixels) placed behind the testing device. The recording time for each frame was 1 s.

After the deformation of the specimen, the surface of the samples was characterized structurally and crystallographically. In order to perform this characterization, a scanning electron microscope (SEM)[1] with a field emission gun operated at 15 kV was used. The microscope was equipped with a detector for the imaging of backscattered electrons (BSE imaging). The EBSD patterns were then recorded and evaluated by an EDAX/TSL EBSD

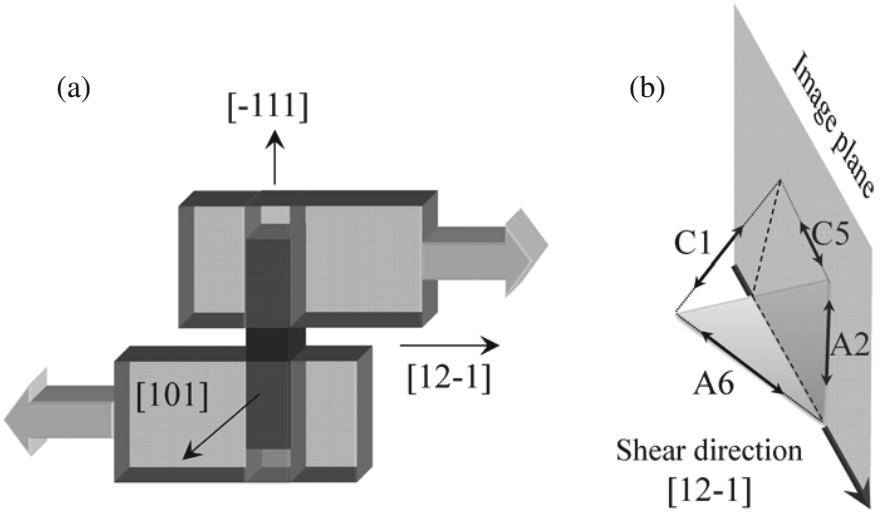

Fig. 8.1 **a:** Specimen in the specimen holder. **b:** Illustration of the crystallographic orientation of the specimen, displaying the slip systems (according to the Schmid-Boas nomenclature (also used in [OR99]). From [DSDR10], © IOP Publishing. Reproduced by permission of IOP Publishing. All rights reserved.

[1] The device used was a JEOL JSM 6500F microscope.

System equipped with a Digiview camera. In the high-resolution EBSD measurements the exposure time for each frame was set to about 0.5 s at the smallest binning size, and for the calculation of the Hough transformation a binned pattern size 240 × 240 and an angular spacing control of 0.5° were chosen.

8.3.3 Outcome of the Single Crystal Shear Deformation Experiments

Shear Deformation and DIC Analysis: The specimens were deformed in simple shear up to a deformation of $\gamma = 0.23$ as measured in the machine extensometer. The load/displacement dependence was recorded during the shear deformation, the data can be seen in Fig. 8.2a. The digital images of the initial and final deformation state as captured for DIC are shown in Fig. 8.2b. A closer inspection of the DIC data of the deformed sample revealed some strain concentration in the sample near the clamps and a large central region of homogeneously deformed material.

This homogeneously deformed part of the sample was then examined more closely. In particular, we found that it can be very well approximated by a completely homogeneous deformation in simple shear with a shear magnitude of $\gamma = 0.20$, but with a normal of shear rotated clockwise by $\varphi = 4.5°$ from the vertical direction.

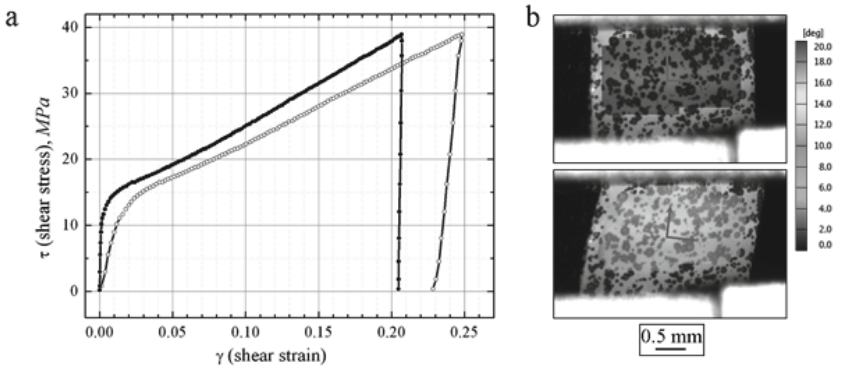

Fig. 8.2 a: Stress/shear angle dependence obtained from the load/displacement measurement (grey curve) and using the DIC method (black curve). **b:** Digital images of the sample surface decorated for the DIC method before (upper image) and after the deformation (lower image). Image from [DDMR09], © Elsevier. Reproduced by permission of Elsevier. All rights reserved.

Microstructural Characterization of the Sample: As mentioned above, the specimen was analyzed in an SEM after deformation. The BSE micrograph of the single crystal sample is shown in Fig. 8.3a, with the direction of the applied shear load indicated by the white arrows. Some glide bands can be observed; their orientation in relation to the nearest plane trace of a {111}-plane is indicated by a grey line. The central area containing the glide bands was then analyzed using EBSD.

Fig. 8.3b shows the EBSD image of the deformed part of the crystal recorded with a step size 2 µm. The mismatch of orientation to the orientation of an arbitrarily chosen point in the image is plotted. One can observe a variation of the orientation within 3°. The formation of a microscopic band structure with a different orientation compared to the material in between the bands can be observed from this map. The averaged orientation of the sample in the image was used to calculate the the plane traces of the {111}-slip planes displayed in the upper right hand corner of the image. The plane trace of the {111}-slip plane containing the two slip systems with maximal modulus of the Schmid factor (as illustrated in Fig. 8.1 above) is shown as a black line in the center of the image. Comparing this direction with the orientation of the microbands (illustrated by the grey line), a deviation of approximately 7° can be determined. Note that the orientation of the microbands is *not* crystallographic. A further feature of the generated bands is

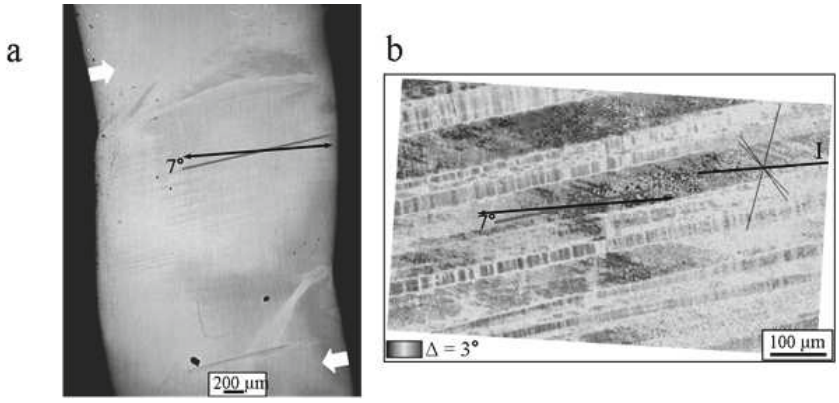

Fig. 8.3 **a:** BSE overview micrograph with white arrows indicating the applied shear load. The black line is a plane trace of a slip-plane (i.e., a {111}-plane). **b:** EBSD characterization of the local lattice orientation. The band-like structure can be clearly observed here. In the upper right corner of the image, the set of {111}-plane traces is displayed, and in the center the orientation of the laminates with respect to the nearest {111}-plane trace is shown. The 7° mismatch between the two is characteristic for the microstructure. From [DDMR09], used with permission.

the additional substrcuture inside of the microbands (which are subdivided by orthogonal lines). For an analysis of this substructure see section 8.3.5.

A high-resolution EBSD image is shown in Fig. 8.4a, taken with a step-size of 0.1 μm. Again, this image presents the local deviation of the orientation with respect to a reference orientation. The grey scale displays that the crystal lattice inside of the microbands is rotated by 3° in comparison to the material outside. Fig. 8.4b, on the other hand, demonstrates the variation of the the crystal orientation out of the defined crystallographic direction, which is nearly parallel to the normal of the frontal face. The grey scale range is the same as in Fig. 8.4a and displays no significant tilt on that order of magnitude. We therefore conclude that the microbands' orientation is rotated 3° clockwise with respect to the outside material and with a rotation axis that is perpendicular to the front face of the specimen.

8.3.4 Energy Minimizing Microstructure

Our hypothesis is that a non-convexity in the energy landscape is the basic mechanism underlying the formation of the patterns described in the previous section. The idea, as pioneered by Ball and James [BJ87], is the following: Consider the deformation of a body from a reference configuration $\Omega \subset \mathbb{R}^3$

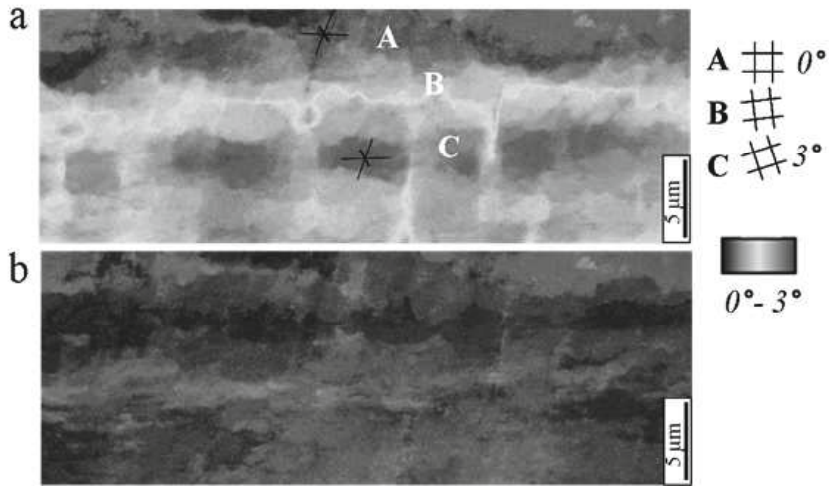

Fig. 8.4 **a:** High resolution EBSD map showing the edge of a microband. The grey scale indicates the the crystal orientation relative to a reference point. A graphical illustration of the observed local lattice rotation is shown on the right hand side. **b:** EBSD map of the same area showing the variation of the orientation away from the normal direction (same scale as above). From [DDMR09], © Elsevier. Reproduced by permission of Elsevier. All rights reserved.

by a sufficiently smooth function $y\colon \Omega \to \mathbb{R}^3$ mapping each point in the reference configuration to its current location. The free energy density of this continuum body is given by a frame indifferent function W depending on the deformation gradient $F = \nabla y$. Assume now that the deformation admits two preferred states (energy minima) F_1 and F_2. Due to material frame indifference, the energy must not change under rigid body motions, i.e., $W(F) = W(QF)$ with $Q \in SO(3)$. Assuming the body is elastically rigid, a good free energy functional can be written as

$$W(F) = \begin{cases} 0 & \text{if } F = QF_1 \text{ or } F = QF_2 \text{ for } Q \in SO(3), \\ \infty & \text{otherwise.} \end{cases} \tag{8.3}$$

A natural question to ask now is which boundary conditions such a material can accommodate in an averaged sense. After relaxing the elastic rigidity to a strong growth away from the minima, one can also introduce small boundary layers in the deformation. In general, this is an open question. However, it is possible to give an interesting upper bound for the relaxation of such a non-convex W. If one assumes that there exists an invariant plane between the two minimizers of the energy, i.e., a plane that is deformed in the same way by both deformation gradients, then one can alternate these two deformation gradients to form a fine scale mixture known as a laminate. The condition for this can be written in the following way: There must exist $Q \in SO(3)$ and $a, n \in \mathbb{R}^3$ such that

$$QF_1 - F_2 = a \otimes n. \tag{8.4}$$

In other words, modulo a rigid body motion, the difference between the deformation gradients must be a rank one matrix. Under these conditions, it is possible to find a *continuous*, *piecewise affine* deformation y whose gradient is at any point given either by QF_1 or F_2. Alternating these deformations with volume fraction λ and $1 - \lambda$ results in affine boundary conditions of the form $\lambda QF_1 + (1 - \lambda)F_2$ that can be accommodated by the material. This situation is illustrated in Fig. 8.5.

To this end, we first determine the macroscopic strain of the sample, which will act a side condition to minimizing an elasto-plastic energy functional. An analysis of the DIC-measurement illustrated in Fig. 8.2 revealed a central, homogeneously deformed section of the specimen with measured macroscopic strain

$$U = \begin{pmatrix} 0.9555 & -0.0198 & 0.0445 \\ & 1.1036 & 0.0198 \\ & & 0.9555 \end{pmatrix} \tag{8.5}$$

in the final deformation state. This calculation of the average strain assumed that the deformation in the direction normal to the crystal surface was the identity. Apart from this we only performed a basis change from the basis used in the DIC measurement to the basis of the f.c.c. lattice.

Subsequently, a MATLAB program was employed to find a deformation that satisfies the twinning equation (8.4) with the two deformation gradients

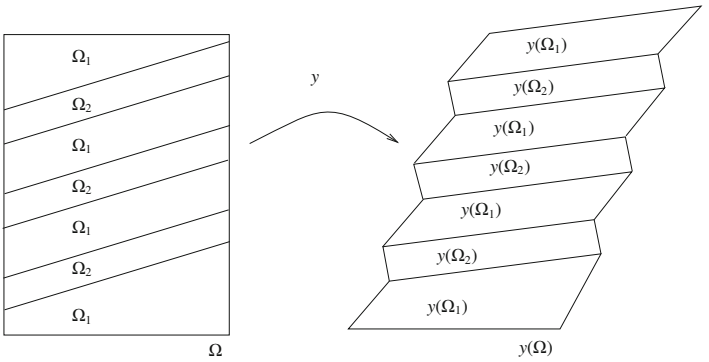

Fig. 8.5 Lamination of a piecewise affine deformation: the two subdomains, Ω_1 and Ω_2, are deformed in an affine manner such that the resulting deformation y is continuous. From [DDMR09], © Elsevier. Reproduced by permission of Elsevier. All rights reserved.

being simple shear in f.c.c. slip systems, while averaging to the strain (8.5) from the measurement. The program simply employs a gradient flow method for the magnitudes of slip in two specifically chosen slip systems with respect to the elasto-plastic energy

$$E = \left\| \sqrt{(UP^{-1})^{\mathrm{T}} \cdot (UP^{-1})} - \mathrm{Id} \right\|^2, \tag{8.6}$$

where $P = (1-\lambda)Q(\gamma_1 P_1 + \mathrm{Id}) + \lambda(\gamma_2 P_2 + \mathrm{Id})$. Here, λ is the volume fraction of one part of the laminate, P_1 and P_2 are the displacement gradients of the two chosen slip systems, and Q is the lattice rotation as calculated in the twinning equation (8.4). Equation (8.6) can be seen as a relaxation of the energy in (8.3) allowing for elastic deformation.

As the main component P_1 of plastic deformation we choose an equal activity in the A2 and A6 slip systems (in the following, we refer to slip systems by the Schmid-Boas nomenclature, also used in [OR99]). We note that these slip systems are naturally compatible without a lattice rotation—they are coplanar slip systems. Following [AD14], we thus consider coplanar slip systems to be lumped into one.

For the secondary component of plastic deformation, there are a number of different choices for a kinematically compatible complementary slip activity. Noting that we are solely looking for a low energy state, we restrict our investigation to two particular possibilities, which guarantee kinematic compatibility independently of the choice of γ_1 and γ_2: first, an equal activity in C1 and C5, and second, an equal activity in B4 and D4.

Which volume fraction is attributed to which slip is a further degree of freedom in our construction. Using the histogram of the distribution of lattice rotations on the whole homogeneously deformed part of the face of the

crystal, we determined that one component of the microstructure occupies approximately two thirds of the total area in the picture. This larger area can now be associated with either the primary component or with the secondary component of the plastic deformation. Note that from the experiments alone, we can not determine this directly, since only the lattice orientation, and not the shear strain was measured microscopically.

We note that if we find such a laminate as described above that also results in a small energy E in (8.6), we immediately have found a deformation state that admits a small energy in the plastic deformation model (8.1) with non-convex dissipation of type (8.2) which averages to the given macroscopic deformation. The reason is the following: the laminate of consisting of two different plastic deformation states as constructed above is automatically admissible with vanishing energy for (8.2). Furthermore, since the laminate is itself a gradient (modulo rigid body motions), it does not require any elastic strain to be made compatible. The only elastic strain appearing in (8.1) is thus the strain from the inexact recovery of the given average strain, i.e., the strain in the energy E in (8.6).

The parameters of the energy minimizers determined by the gradient flow are displayed in Table 8.1. It can be observed that some of the slip-system combinations yield lamination parameters (i.e., direction of the lamination normal, and relative lattice orientation) matching very well the experimental data. The resulting deformations are illustrated in Fig. 8.6, to be compared with the EBSD-results.

Table 8.1 Results from the energy minimization algorithm used to find a low energy laminate of slip systems recovering the average strain in (8.5). The value of λ is the volume fraction of slip in P_2. The values γ_i are the amount of slip in the respective slip system, α is the (clockwise) angle of orientation of the lamination normal with respect to the nearest $\langle 111 \rangle$-direction. The value β is the (clockwise) angle of lattice misorientation. The value E is the energy at the minimizing state. All rotations are exactly in the plane with normal [101].

Choice of slip systems	λ	γ_{P1}	γ_{P2}	α	β	E
$P_2 = \text{B4+D4}$	1/3	0.18	0.082	-7.5°	3.8°	$5.0 \cdot 10^{-6}$
$P_2 = \text{C1}-\text{C5}$	2/3	0.28	-0.040	-6.3°	3.3°	$5.0 \cdot 10^{-6}$

8.3.5 An Analysis of the Substructure Within the Lamination Bands

In Fig. 8.3 one can clearly see the formation of a substructure within the microbands of an orientation variation of 1°. The reasons for the formation of this substructure were examined in [DSDR10]. There, a discrete dislocation dynamics model was used to determine the equilibrium distribution of

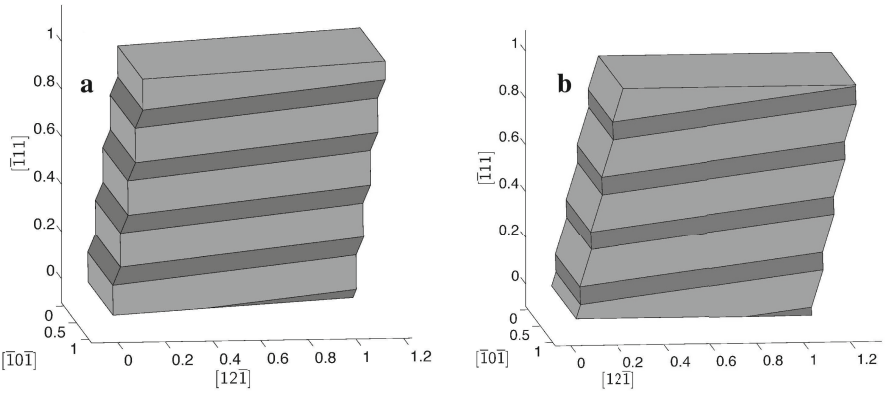

Fig. 8.6 Illustration of the two laminates from Table 8.1 that agree well with the EBSD result from Fig. 8.3b. From [DDMR09], © Elsevier. Reproduced by permission of Elsevier. All rights reserved.

dislocations within the microbands. Given the boundary conditions of bending near the clamped edges of the specimen, the formation of domain walls within the microbands in quantitative agreement with the observed orientation variation was found.

8.4 Conclusions

Here we presented the findings of a copper single crystal shear experiment as published in [DDMR09, DSDR10], in relation to modeling plasticity microstructure by variational approaches. These experiments show that the theory of kinematically compatible microstructures, in particular laminate microstructures, can indeed be used to predict the formation of microstructure in plasticity. We demonstrated that there exist low-energy states consisting of plastic laminates whose macroscopic deformation averages to the measured macroscopic strain, while at the same time their microstructural properties do match the measured properties of the local lattice orientation patterning. In this sense, our work justifies the energy minimization approach to plasticity used for example in [CDK13b, CDK13a, CDK11, ACD09, CDK09, HHK12, HK11, KH11].

A main question that remains open regards the evolution of such laminate microstructures, in particular, whether those structures can arise in finite-strain deformation, where the lamination normal depends on the amount of shear. Some ideas for modeling the evolution of laminates have been explored in [KH11]. In this particular case, we see that during the course of the deformation, only a minor change in the lamination normal was necessary [DDMR09].

Acknowledgements. The authors gratefully acknowledge support from the DFG through the research unit FOR 797 *Analysis and computation of microstructure in finite plasticity*, subprojects P6 and P7.

References

[ACD09] Albin, N., Conti, S., Dolzmann, G.: Infinite-order laminates in a model in crystal plasticity. Proc. Roy. Soc. Edinburgh Sect. A 139(4), 685–708 (2009)

[AD14] Anguige, K., Dondl, P.W.: Relaxation of the single-slip condition in strain-gradient plasticity. Proceedings of the Royal Society of London A: Mathematical, Physical and Engineering Sciences, 470(2169) (2014)

[BHHK92] Bay, B., Hansen, N., Hughes, D., Kuhlmann-Wilsdorf, D.: Overview no-96 – evolution of FCC deformation structures in polyslip. Acta Metallurgica et Materialia 40(2), 205–219 (1992)

[BJ87] Ball, J.M., James, R.D.: Fine phase mixtures as minimizers of energy. Arch. Rational Mech. Anal. 100(1), 13–52 (1987)

[CDK09] Conti, S., Dolzmann, G., Klust, C.: Relaxation of a class of variational models in crystal plasticity. Proc. R. Soc. Lond. Ser. A Math. Phys. Eng. Sci. 465(2106), 1735–1742 (2009)

[CDK11] Conti, S., Dolzmann, G., Kreisbeck, C.: Asymptotic behavior of crystal plasticity with one slip system in the limit of rigid elasticity. SIAM J. Math. Anal. 43(5), 2337–2353 (2011)

[CDK13a] Conti, S., Dolzmann, G., Kreisbeck, C.: Relaxation and microstructure in a model for finite crystal plasticity with one slip system in three dimensions. Discrete Contin. Dyn. Syst. Ser. S 6(1), 1–16 (2013)

[CDK13b] Conti, S., Dolzmann, G., Kreisbeck, C.: Relaxation of a model in finite plasticity with two slip systems. Math. Models Methods Appl. Sci. 23(11), 2111–2128 (2013)

[CG01] Cermelli, P., Gurtin, M.E.: On the characterization of geometrically necessary dislocations in finite plasticity. Journal of the Mechanics and Physics of Solids 49(7), 1539–1568 (2001)

[DDMR09] Dmitrieva, O., Dondl, P.W., Müller, S., Raabe, D.: Lamination microstructure in shear deformed copper single crystals. Acta Materialia 57(12), 3439–3449 (2009)

[DSDR10] Dmitrieva, O., Svirina, J.V., Demir, E., Raabe, D.: Investigation of the internal substructure of microbands in a deformed copper single crystal: experiments and dislocation dynamics simulation. Modelling and Simulation in Materials Science and Engineering 18(8) (December 2010)

[Han90] Hansen, N.: Cold deformation microstructures. Materials Science and Technology 6(11), 1039–1047 (1990)

[HBO10] Hansen, B.L., Bronkhorst, C.A., Ortiz, M.: Dislocation subgrain structures and modeling the plastic hardening of metallic single crystals. Modelling and Simulation in Materials Science and Engineering 18(5), 055001 (2010)

[HHK12] Hackl, K., Hoppe, U., Kochmann, D.M.: Generation and evolution of inelastic microstructures—an overview. GAMM-Mitt. 35(1), 91–106 (2012)

[HK11] Hackl, K., Kochmann, D.M.: An incremental strategy for modeling laminate microstructures in finite plasticity—energy reduction, laminate orientation and cyclic behavior. In: de Borst, R., Ramm, E. (eds.) Multiscale Methods in Computational Mechanics. LNACM, vol. 55, pp. 117–134. Springer, Heidelberg (2011)

[JW84] Jin, N., Winter, A.: Dislocation structures in cyclically deformed [001] copper crystals. Acta Metallurgica 32(8), 1173–1176 (1984)

[KH11] Kochmann, D.M., Hackl, K.: The evolution of laminates in finite crystal plasticity: a variational approach. Contin. Mech. Thermodyn. 23(1), 63–85 (2011)

[Kon52] Kondo, K.: On the geometrical and physical foundations of the theory of yielding. In: Proc. 2nd Japan Nat. Congr. Applied Mechanics, pp. 41–47 (1952)

[MRF10] Miehe, C., Rosato, D., Frankenreiter, I.: Fast estimates of evolving orientation microstructures in textured bcc polycrystals at finite plastic strains. Acta Materialia 58(15), 4911–4922 (2010)

[Nye53] Nye, J.F.: Some geometrical relations in dislocated crystals. Acta Metallurgica 1(2), 153–162 (1953)

[OR99] Ortiz, M., Repetto, E.A.: Nonconvex energy minimization and dislocation structures in ductile single crystals. J. Mech. Phys. Solids 47(2), 397–462 (1999)

[RC14] Reina, C., Conti, S.: Kinematic description of crystal plasticity in the finite kinematic framework: a micromechanical understanding of $F = F^{\mathrm{e}}F^{\mathrm{p}}$. J. Mech. Phys. Solids 67, 40–61 (2014)

[RP80] Rasmussen, K., Pedersen, O.: Fatigue of copper polycrystals at low plastic strain amplitudes. Acta Metallurgica 28(11), 1467–1478 (1980)

[RP99] Rodney, D., Phillips, R.: Structure and strength of dislocation junctions: An atomic level analysis. Physical Review Letters 82(8), 1704–1707 (1999)